Magnetic Resonance in Chemistry

WILEY

RESEARCH ARTICLE OPEN ACCESS

NMR Relaxometry to Monitor In Situ the Loading of Amberlite IR120 and Dowex Marathon MSC Resins With Ni^{2+} and Cu^{2+} During a Column Experiment

Marie Bernardi[1] | Rodrigo de Oliveira Silva[2] | Quoc Lam Vuong[1] | Dimitrios Sakellariou[2] | Yves Gossuin[1]

[1]Biomedical Physics Unit, Research Institute for Materials Science and Engineering, UMONS, Mons, Belgium | [2]Centre for Membrane Separations, Adsorption, Catalysis and Spectroscopy (cMACS), KU Leuven, Leuven, Belgium

Correspondence: Yves Gossuin (yves.gossuin@umons.ac.be)

Received: 30 August 2024 | **Revised:** 1 October 2024 | **Accepted:** 2 October 2024

Funding: This work was supported by Fonds De La Recherche Scientifique - FNRS (Wallonia-Brussels Federation, Belgium) grants (grant numbers T.0113.20, CDR J.0093.22, and CDR J.0025.15).

Keywords: benchtop NMR | column experiment | copper | heavy metal ions removal | ion exchange | nickel | NMR relaxometry | relaxation

ABSTRACT

The removal of heavy metal ions from wastewater often necessitates the use of ion exchange resins. Current methods for assessing ion exchange efficiency are indirect and destructive. Some heavy metal ions, such as Cu^{2+} and Ni^{2+}, are paramagnetic and influence the NMR relaxation times of water protons. NMR relaxometry can therefore be utilized to track the removal of these ions by ion exchange resins. In this study, we use relaxometry to monitor in situ the loading with Ni^{2+} and Cu^{2+} of Amberlite IR120 and Dowex Marathon MSC resins, with the resin column inserted into a low-field NMR device. The multiexponential transverse relaxation curves were fitted using a biexponential model. Before and during the loading of the resin, the water with the slowest relaxation corresponds to treated water (free of Ni^{2+} or Cu^{2+}) flowing between the resin beads. After saturation, the slowest fraction corresponds to the untreated solution (containing Ni^{2+} or Cu^{2+}) flowing between the resin beads saturated with paramagnetic ions. The evolution with time of the transverse relaxation rate and the amplitude of the slowly relaxing water fraction shows a clear transition, occurring later at the bottom of the resin bed compared with the middle and top. This is interpreted as an indication of the saturation of the studied zone with paramagnetic ions, confirmed by the quantification of Ni^{2+} or Cu^{2+} in the effluent using AES spectroscopy. This proof-of-concept study demonstrates that NMR relaxometry can be used in situ to monitor the loading of a resin bed with paramagnetic ions.

1 | Introduction

The presence of heavy metal ions in water is a major environmental issue. Copper ions, for example, are found in wastewater from electric, electronic, electroplating, and tanning industries, whereas nickel ions are released by metal mining, nickel plating, and alloy manufacturing industries, as well as during the combustion of fossil fuels [1–3]. Exposure to high concentrations of both copper and nickel ions can cause severe health problems, which is why their concentrations in drinking water must be minimized. The World Health Organization (WHO) recommends a maximum concentration of 2 mg/L (30 μM) for copper and 0.07 mg/L (1.2 μM) for nickel in drinking water [4]. Various methods exist for removing these ions

Abbreviations: NMR, nuclear magnetic resonance; MRI, magnetic resonance imaging.

from water, including chemical coprecipitation, adsorption, and ion exchange [5–8], each with its own advantages and disadvantages in terms of cost, efficiency, and reusability. Ion exchange uses resins that exchange their cations (e.g., H^+ and Na^+) with metal ions present in wastewater.

To study the removal efficiency of a compound, batch or column experiments can be performed, followed by atomic absorption/emission spectroscopy (AAS and AES) on the supernatant (for batch experiments) or on the outlet effluent (for column experiments). In a column experiment, the results are often presented as a breakthrough curve, which represents the outlet effluent metal concentration as a function of time. At the beginning of the curve, the outlet metal ion concentration is zero because the column captures all the heavy metal ions from the solution. At the end of the experiment, when the resin is saturated with metal ions, the outlet concentration equals the inlet concentration. Live recording of a breakthrough curve is currently not possible, as the metal concentration in the effluent is only determined after elemental analysis by AAS or AES, which sometimes requires acid digestion. A technique that allows for real-time monitoring of resin loading directly in the column during the experiment would therefore be valuable. Evaluating the loading of the resin bed during operation would also help to decide when the resin must be changed, before metal ions appear in the effluent.

Ni^{2+} and Cu^{2+} ions are paramagnetic, enabling their detection by NMR relaxometry [9, 10]. Their presence in water accelerates the magnetic relaxation of water protons. This principle has been used to follow Ni^{2+} distribution in porous media using MRI [11]. Fe^{2+}, Co^{2+}, and Gd^{3+} transport in methanogenic granules has also been studied by MRI [12]. The propagation of paramagnetic tracers in columns containing sandy aquifer matrices or other porous media has been successfully observed by MRI [13–15]. More recently, we proposed using NMR relaxometry in batch experiments to study the adsorption of Cu^{2+} on alumina [16] and the ion exchange of Cr^{3+} and Cu^{2+} by Amberlite IR120 (Na^+) resin [17]. Marchesi et al. [18] used a similar approach to study the removal of Gd^{3+}, Cu^{2+}, and Co^{2+} from water using saponite clay. The capture of Ni^{2+} ions by Amberlite IR120 (Na^+), Amberlite IRC748 (Na^+), Dowex Marathon MSC (H^+) resins, and activated charcoal has also been studied by relaxometry [19]. In addition to conventional batch experiments—where the NMR signal originates from the supernatant water protons—the relaxation properties of the sorbent/resin loaded with paramagnetic ions were also studied [16, 17, 19]. In these experiments, the signal originates from the water present in the intergranular and intragranular porosity of the packed adsorbent. A strong correlation was found between specific relaxation parameters and the actual metal content of the sorbent/resin. This paved the way for using NMR relaxometry directly on the sorbent/resin bed in column experiments, aiming to monitor in situ the gradual loading of the resin with paramagnetic ions.

In this work, we studied the capture of Cu^{2+} and Ni^{2+} by Amberlite IR120 (Na^+) and Dowex Marathon MSC (H^+) during column experiments, using NMR relaxometry with the column directly inserted into the bore of the NMR system. Our results demonstrate that monitoring paramagnetic ion exchange during a column experiment is feasible, although the methodology will need to be adapted to more realistic conditions.

2 | Material and Methods

2.1 | Samples

Two strongly acidic cation exchange resins, Amberlite IR120 and Dowex Marathon MSC (Sigma-Aldrich), were investigated. Their main characteristics are provided in Table 1. The resins were selected due to their structure (gel or macroporous) and their affinity for Cu^{2+} and Ni^{2+}. The solutions of Ni^{2+} and Cu^{2+} were prepared by dissolving nickel nitrate hexahydrate and copper sulfate pentahydrate, respectively, in deionized water. All reagents were purchased from Sigma-Aldrich.

2.2 | Column Experiment

A sketch of the experimental setup is provided in Figure 1a along with a picture of the column inside the NMR magnet in Figure 1b. The setup of the column experiment and the parameters used (paramagnetic ion concentration, flow rate, mass of resin, etc.) were inspired from previous studies [20–23]. The experiments were performed in continuous flow using a fixed-bed glass column with an internal diameter of 2 cm and a height of 80 cm. A sintered glass disk with porosity P0 was used at the bottom of the column to prevent the loss of column content. A mixture of 64.5 g of 2-mm glass beads (VWR) and distilled water was added to the column to position the resin bed in the 3-cm-high detection zone of the NMR system. Then another sintered glass P0 porosity disk was inserted to level the bottom of the resin pack. The "slurry" packing method was used: Distilled water was added to the wet resin in a beaker before being carefully poured along the inside wall of the column to prevent air being trapped in the slurry. Finally, we added a sintered glass P0 porosity disk above the resin bed, then glass beads before finishing the assembly with a last sintered glass disk. These elements level the top of the resin pack. At every stage of filling, the entrapped air was removed by connecting the top of the column to a vacuum pump and keeping the column outlet closed for a few minutes. Meanwhile, a glass rod was used to tap the column to help remove air bubbles. The mass of resin (14 g for IR120 and 12.3 g for Marathon MSC) was chosen to obtain a height of 5 cm for the resin bed. The solution containing nickel and copper ions, with a 20-mM concentration, was fed to the top of the column using a peristaltic pump (Preciflow, Lambda Laboratory Instruments) to control the inlet flow rate (4.3 mL/min). The choice of this relatively high concentration was made to keep the experiment time reasonable (a few hours). Indeed, using lower concentrations, although more realistic, would require several days for a single column experiment, which would be difficult to set up. A 67-cm silicon tube connects the column outlet to a tap, which opens and closes the outlet flow. During the experiment, the solution was maintained at a constant level in the column by adjusting the outlet flow rate to the inlet flow rate. The speed of the liquid in the resin bed can be estimated thanks to the flow rate and the diameter of the column, which provides a speed of 14 mm/min. Outlet fractions were collected

TABLE 1 | Physico-chemical properties of the two studied resins.

	Amberlite IR120	Dowex Marathon MSC
Matrix	Styrene-divinylbenzene	Macroporous styrene-divinylbenzene
Functional group	Sulphonic acid	Sulphonic acid
Ionic form	Na^+	H^+
Particle size	0.60–0.80 mm	0.525–0.625 mm
Moisture	40%–50%	50%–56%
Total exchange capacity	≥ 2.00 eq/L	1.60 eq/L

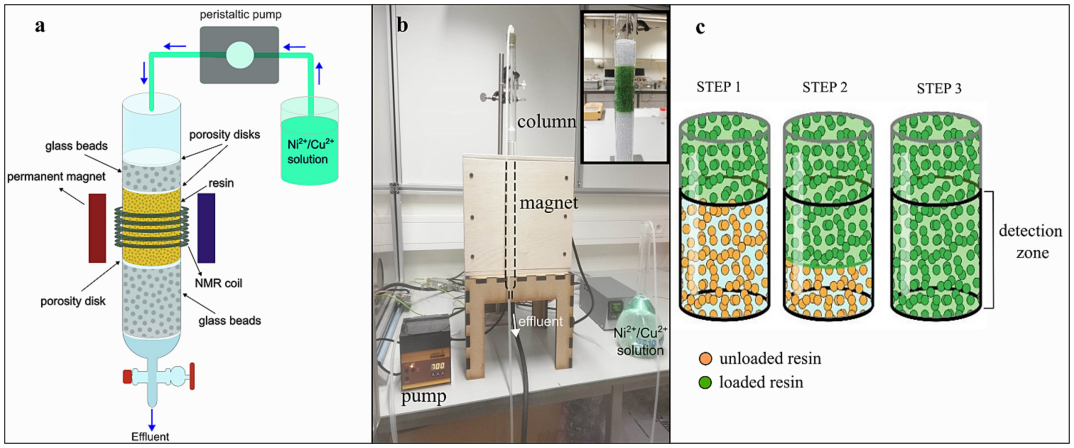

FIGURE 1 | (a) Sketch of the experimental setup. (b) Picture of the actual experiment. The inset shows a close-up of the column after saturation with Ni^{2+}. (c) Sketch of the gradual loading of the resin bed with paramagnetic ions.

for 1 min every 15 min, and their concentrations were subsequently measured by AES. The experiment is designed so that the solution is not collected immediately after passing through the resin pack; instead, it is collected after passing through 14 cm of glass beads inside the column and the silicone tube of 67 cm with an internal diameter of 1 cm. Knowing the flow rate, diameter, and length of the column/tube, we can estimate the delay between the time the solution gets out of the resin pack and when it is finally collected. This delay is estimated to be around 17 min and is considered when comparing direct NMR measurements with indirect AES measurements performed on the effluent collected fractions. To monitor the ion exchange process at different levels of the resin bed, the whole column was simply moved up or down in the coil of the NMR system, allowing the study of the upper part (3 cm of the top), the middle part (3 cm in the middle), and the lower part (3 cm at the bottom) of the resin bed.

2.3 | NMR Relaxometry

Relaxation experiments were performed in a 196-mT permanent magnet assembly with a free bore of 3 cm in diameter, thermalized to 28°C. The corresponding proton Larmor frequency is 8.33 MHz. The magnet and probe were built by the RE Magnet Studio Ltd. following the design of a pseudo Halbach dipole [24]. The column was inserted in the bore of the magnet and centered to position the resin bed at the sweet spot of the magnet. The height of the zone excited and detected by the coil is estimated to be ~3 cm centered on the sweet spot of the magnet. A Scout/Tecmag spectrometer console was used together with a BLAX/Bruker 300-W radio-frequency amplifier.

T_2 was determined using the CPMG sequence. Eighteen thousand echoes, equally spaced by 300 µs, were recorded for a total echo train length of 5.4 s. For each echo, the 32 central complex points were stored with a dwell time of 2 µs, corresponding to a spectral window of 500 kHz. The effect of the flow during the CPMG measurement can be neglected. Indeed, the displacement of water between the excitation and the last echo of the CPMG train is 1.3 mm, whereas the total height of the studied zone is 3 cm. The number of scans was equal to 8 and the repetition delay was put to 6 s. The total acquisition time for each T_2 in this kinetic study was 91 s. This acquisition time is small when compared with the time needed for the saturation of the column, which requires several hours. Thus, the measurement of T_2 is sufficiently fast to follow the loading of the column with paramagnetic ions.

In some experiments, T_1 was also measured just after the T_2 determination. The inversion recovery sequence was used. The signal after the 90° recovery pulse was obtained with a truncated CPMG sequence with an interecho time of 300 μs, recording only the first 10 echoes. The length of the echo train was thus 3 ms. For each echo, the eight central complex points were stored with a dwell time of 2 μs (500 kHz spectral window). The number of scans was equal to 4, and the repetition delay was put to 6 s. The recovery delay was logarithmically incremented from 100 μs to 10 s in 16 steps. The effect of the flow is more significant for T_1. Indeed, the displacement of the liquid in the resin bed between the excitation and the detection for the longest delay of the inversion recovery is estimated at 2.4 mm, which represents ~10% of the measured zone. The total acquisition time for each T_1 was ~7.5 min, which is also much longer than for T_2.

2.4 | Fitting of the Relaxation Data

The relaxation curves obtained for the water protons contained in the resin bed are not monoexponential but multiexponential curves. This is because several fractions of water protons coexist in the column, each corresponding to a specific relaxation rate. The amplitude of each exponential is proportional to the corresponding amount of water protons. For most of the curves, a biexponential fitting of the relaxation curves was satisfactory (R^2 larger than 0.8), with a slowly and a fast-relaxing fraction. Depending on the stage of resin loading with the paramagnetic ions, the amplitude and relaxation rate of the proton fractions evolve. Let us focus, for example, on the bottom of the resin bed. To describe the system, one must consider three consecutive steps for this zone of the resin bed: before the loading of resin with paramagnetic ions (step 1), during the loading of resin with paramagnetic ions (step 2), and after the loading of resin with paramagnetic ions (step 3). These three steps are illustrated in Figure 1c.

During step 1, before the beginning of the loading of the studied zone, two water fractions can be easily identified. The fast-relaxing fraction corresponds to water trapped in the unloaded resin, whereas the slow-relaxing fraction corresponds to pure water (without paramagnetic ions) flowing between the resin beads. Indeed, before the loading of the bottom of the resin bed, the solution reaching the zone has already been treated by the resin situated above, which means that all the paramagnetic ions have already been captured. The relaxation of the water contained inside the resin is faster than that of pure water, as expected for porous media [25]. During this step, a biexponential analysis of the data provides good results.

During step 3, after the complete loading, the solution flowing in the zone has not been treated, because all the resin above the studied zone and inside the studied zone is already saturated. This means that the concentration of paramagnetic ions in the flowing solution is the same as in the feeding solution (20 mM). The protons of this fraction contribute to the slow fraction of the biexponential curves. The protons belonging to water trapped inside the resin saturated with paramagnetic ions experience very fast relaxation, corresponding to the fast fraction during this step. Here also, a biexponential analysis is appropriate. It is interesting to note that the amplitude of the slow fraction is expected to be the same as in step 1. In both cases, the slow fraction corresponds to water situated between the resin beads.

During step 2, corresponding to the loading of the studied zone, four populations of protons potentially coexist: pure water (without paramagnetic ions), water containing paramagnetic ions, water inside the unloaded resin, and water inside the resin loaded with paramagnetic ions. However, for the sake of simplicity, we decided to use a biexponential fitting of the relaxation data during this intermediate step as well. As will be shown later, the biexponential analysis misses the initial very fast fraction, which corresponds to water trapped in loaded resin. The slow fraction of the biexponential fitting is attributed to water without or with small amounts of paramagnetic ions. The fast fraction corresponds to water with a high concentration of paramagnetic ions and water in unloaded resin. This is clearly a very simplified approach: More than two exponentials could have been used. However, the convergence of such fittings with more than two exponentials can be problematic and the errors on the fitting would be significant. This is what we observed when we tried to treat our data with triexponential fittings. We therefore decided to use the simplest approach with a simple biexponential fitting for this intermediate region as well. The results obtained during this intermediate step must be interpreted more cautiously because of these fitting issues. However, because we will focus on the slowly relaxing fraction, the interpretation will be simplified. Indeed, this fraction corresponds to water without or with only small amounts of paramagnetic ions that flows between the beads. In this fraction, there is no contribution from the water contained inside resin.

The fitting procedure and the interpretation of the different fractions of protons is valid for transverse relaxation. However, we noticed that the interpretation of the biexponential fittings was less straightforward for longitudinal relaxation curves. Indeed, the number of points recorded for T_1 curves is much smaller than for T_2 curves, especially for very short delays, which complicates the fitting and the interpretation of the T_1 curves.

The biexponential function used for the fitting of the transverse relaxation curves was

$$S(t) = S_0\left[A_{fast}e^{-t/T_{2,fast}} + A_{slow}e^{-t/T_{2,slow}}\right] \quad (1)$$

where S_0 is the signal extrapolated at $t = 0$, A_{fast} and A_{slow} are the normalized amplitudes of the fast and slow proton fractions, respectively ($A_{\text{fast}} + A_{\text{slow}} = 1$), and $T_{2,\text{fast}}$ and $T_{2,\text{slow}}$ are the transverse relaxation times of the fast and slow fractions, respectively. In the different graphs, the errors on the amplitudes and relaxation rates are the errors provided by the fitting.

To obtain the T_2 relaxation times distributions, the raw transverse relaxation curves were processed with a

homemade inverse of Laplace transform (ILT) using CONTIN algorithm [26].

3 | Results

3.1 | Example of the Loading of an Amberlite IR120 Resin Bed With Ni^{2+}

3.1.1 | Raw Transverse Relaxation Curves

Figure 2a–c shows the curves of return to equilibrium of transverse magnetization obtained respectively before (step 1), during (step 2), and after (step 3) the loading of the IR120 resin with Ni^{2+} ions, at the bottom of the resin bed. The curves are clearly multiexponential. The line represents the fittings of the relaxation data with a biexponential function, which provides the relaxation rates and the relative amplitudes of the fast and slowly relaxing fractions, as described in Section 2 (Equation 1). The biexponential fitting of the relaxation data is satisfying for the relaxation curves obtained before and after the loading of the resin, as shown in Figure 2a,c. Between these, that is, during the loading, it is clear from Figure 2b that there are more than two populations of protons. The fastest fraction, with a relaxation time of a few milliseconds, is not considered in the fitting. It corresponds to water contained inside resin beads loaded with Ni^{2+} ions. Nevertheless, for the sake of simplicity, we also use biexponential fittings for the data corresponding to the loading of the resin bed. For these intermediate times, the parameters obtained by the biexponential fitting must be interpreted a bit more cautiously, especially those concerning the fast-relaxing fraction.

3.1.2 | Typical Evolution of the Relaxation Rate and Amplitude of the Slowly Relaxing Fraction

In this section, we describe in detail the time evolution of the relaxation rate and amplitude of the slow fraction during the column experiments, using the example of the capture of Ni^{2+} ions by the IR120 resin with the NMR detection zone located at the bottom of the resin bed. Figure 3a shows the evolution over time of $1/T_2$ of the slow fraction of the biexponential fitting. The corresponding evolution for the normalized amplitude of this fraction is presented in Figure 3b.

In the first part of the curve (step 1), before the loading of the resin, $1/T_{2,slow}$ is ~$0.6\,s^{-1}$, which is consistent with pure water flowing between the beads. This value is a bit larger than what is expected for pure water (~$0.5\,s^{-1}$), but this difference could be explained by the effect of the difference of magnetic susceptibility between the beads and water, which could result in a slightly faster transverse relaxation in the interporosity. During this first step, the normalized amplitude of the slow fraction, A_{slow}, is around 0.6 (Figure 3b). The fast fraction corresponds to protons belonging to water molecules trapped in the intraporosity of the resin beads, with a normalized amplitude A_{fast} ~0.4 and a transverse relaxation rate $1/T_{2,fast}$ ~$1.8\,s^{-1}$ (Figures S1 and S2).

In the final part of the curve (step 3), $1/T_{2,slow}$ is ~$13.5\,s^{-1}$, which is 10% larger than the relaxation rate of a 20-mM Ni^{2+} solution measured in the same conditions, $1/T_2 = 12.2\,s^{-1}$ (dashed line in Figure 3a). This slightly faster relaxation of the 20-mM Ni^{2+} solution when it is confined in the interporosity of the resin bed could be explained by susceptibility effects, because the magnetic susceptibility of the resin and of the solution present in the interporosity are different. The normalized amplitude of the slow fraction A_{slow} is ~0.6, which is the same as in the first part of the curve (step 1). It is consistent: In both cases, this fraction corresponds to protons belonging to water molecules present between the resin beads, in the interporosity, whose volume is the same in step 1 and 3. During step 1, it is filled with pure water, whereas, during step 3, it is filled with a 20-mM Ni^{2+} aqueous solution. The fast-relaxing fraction of protons, corresponding to water molecules contained inside the resin beads, present a very large relaxation rate $1/T_{2,fast}$ ~$630\,s^{-1}$ (Figure S2). The amplitude of this fast fraction is 0.4 (Figure S1), which corresponds to the amount water molecules protons in the intraporosity of the resin, as during step 1. The only difference is that the resin beads are now saturated with Ni^{2+} ions. In a previous study [19], we showed that $1/T_2$ for water inside Ni^{2+} loaded IR120 resin could reach $500\,s^{-1}$ for high Ni^{2+} content ($32\,mg_{Ni}/g_{dry\ resin}$). The value of $1/T_{2,fast}$ is thus in good agreement with what is expected for a saturated resin, whose maximum content in Ni is ~$40\,mg_{Ni}/g_{dry\ resin}$. Indeed, when using the power law reported in our previous study [19], one can predict a value of $1/T_{2,fast}$ ~$670\,s^{-1}$ for the water contained into Ni^{2+}-saturated IR120 resin.

The interpretation of the middle part of the curves (step 2) is less straightforward: $1/T_{2,slow}$ remains smaller than $2\,s^{-1}$ but increases with time, because of the presence of small residual amounts of paramagnetic ions in the treated water flowing between the beads. The amplitude A_{slow} decreases from 0.6 to 0.1, just before jumping back to 0.6 after the complete loading of the resin (beginning of step 3). Indeed, during the loading step, the amount of treated water in the studied zone decreases, which explains the decrease of A_{slow}. The normalized amplitude A_{fast} of the fast-relaxing fraction of protons increases during the loading of the studied zone of the resin bed (Figure S1). It is consistent because in this fraction, one finds the concentrated Ni^{2+} solution that has not yet reached the unsaturated resin bed. As the resin loading progresses, the volume of concentrated solution in the studied area increases, leading to an increase of A_{fast}. The relaxation rate of the fast fraction ($1/T_{2,fast}$) also increases during this second step (Figure S2). As this fraction corresponds to several populations of water protons (water contained in unloaded or slightly loaded resin and untreated water with high concentrations of Ni^{2+} flowing between the beads), $1/T_{2,fast}$ is a mean value and the interpretation of this increase is not straightforward.

The transition between step 1 and step 2 can be seen in Figure 3a,b (blue arrows): When the concentrated Ni^{2+} solution enters the zone studied by NMR, a small discontinuity is observed on the curves: $1/T_{2,slow}$ slightly increases, whereas A_{slow} slightly decreases. The transition between steps 2 and 3 is easily spotted in the graphs because it corresponds to a sudden and large change in both the amplitude and the relaxation rate of the slow fraction. This transition occurs when the zone studied by NMR becomes almost completely saturated. In this situation, there is no more

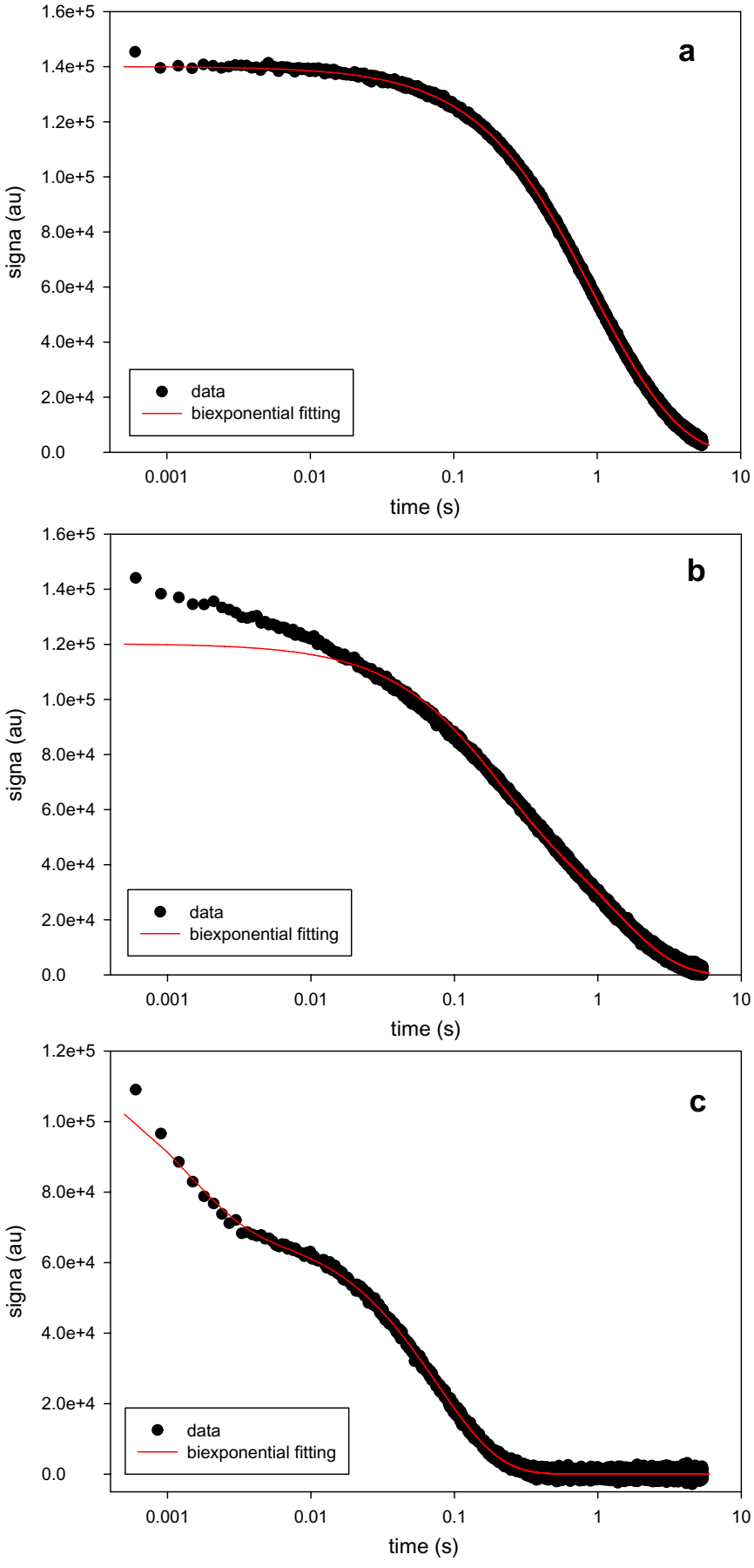

FIGURE 2 | Curves of return to equilibrium of transverse magnetization for the bottom of the column bed (a) before (step 1, $t = 0$ h), (b) during (step 2, $t = 1.88$ h), and (c) after (step 3, $t = 4.7$ h) the loading of IR120 resin with Ni^{2+} ions.

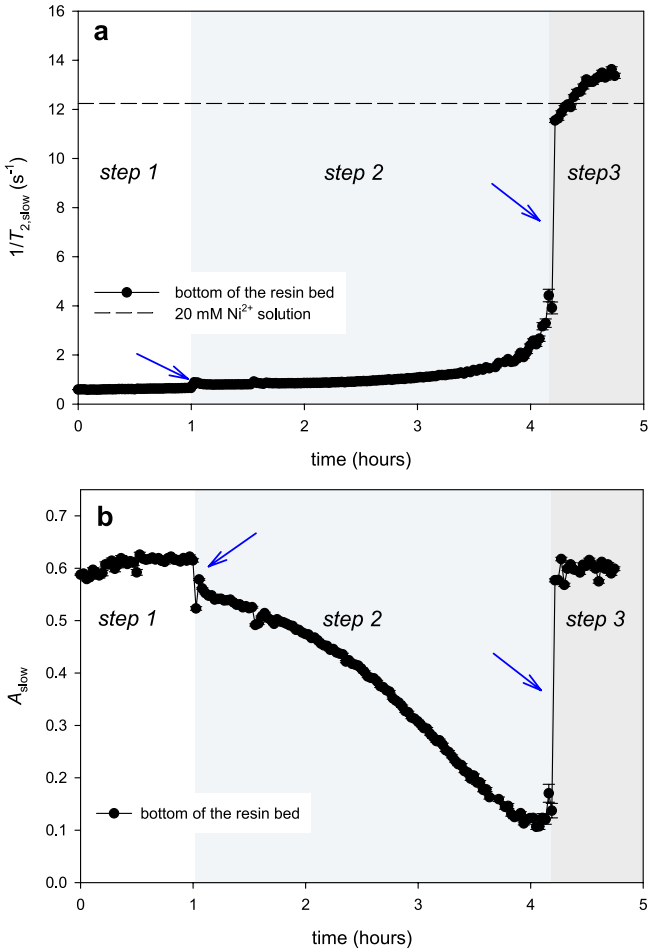

FIGURE 3 | Loading of the bottom of an IR120 resin bed with Ni^{2+} ions. Evolution with time of (a) the transverse relaxation rate $1/T_{2,slow}$ of the slow fraction and (b) the normalized amplitude A_{slow} of the slow fraction obtained by the biexponential fitting of the transverse relaxation data. The blue arrows show the transitions between the different zones of the curves described in the text.

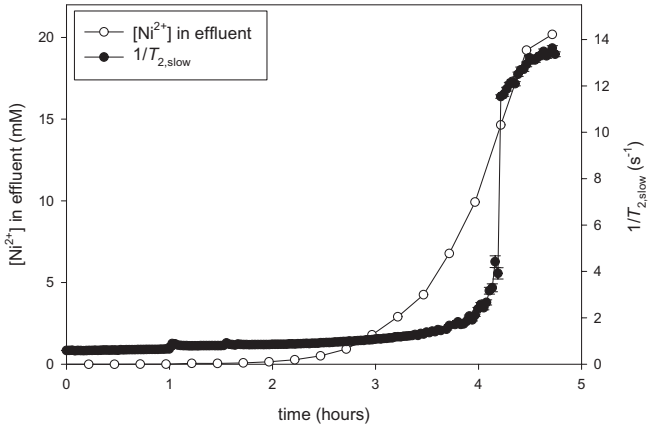

FIGURE 4 | Breakthrough curve of the IR120 resin bed with a 20-mM Ni^{2+} solution, obtained by the measurement of Ni^{2+} concentration in the effluent. The evolution of $1/T_{2,slow}$ for the bottom of the resin bed is also shown for comparison.

pure water in the zone: It is replaced by a concentrated Ni^{2+} solution, which explains the change in relaxation rate and amplitude. We calculate the time needed to reach this transition as the time after which $1/T_2$ of the slow fraction reaches 80% of its maximal value (measured at the end of the experiment). In the case of Ni^{2+} with IR120 resin, the bottom zone of the bed is saturated after 4.22 h. This is confirmed by the breakthrough curve of the column, obtained by the quantification of Ni^{2+} in the effluent at different time intervals. It is presented in Figure 4, together with the evolution of $1/T_{2,slow}$. The abrupt change in the relaxation rate of the slow fraction occurs at the end of the breakthrough curve, when the concentration in the effluent is already 15 mM, which means that the column is almost saturated.

3.1.3 | T_2 Distribution Obtained by Inverse Laplace Transform (ILT)

The relaxation curves were also analyzed with ILT to obtain the evolution with time of the T_2 distribution during the column experiment (Figure 5). The different fractions of water protons described above are clearly present in the distributions. Moreover, the three successive steps of the experiment are also observed, which confirms the interpretation presented in the previous paragraph. The very fast fraction of protons missed by the biexponential fitting during step 2 can be observed on the left of the T_2 distribution. However, the obtained distributions present rather broad peaks whose position seems unstable, as can be noticed in Figure 5. This is probably due to the noise in the relaxation curves. Therefore, we decided to use the T_2 distributions only as a complementary analysis of our data.

3.1.4 | Influence of the Height of the Studied bed Zone

To choose which region of the resin bed was the most appropriate for the follow up of the resin loading with paramagnetic ions, we have carried out three experiments with different positioning of the column inside the NMR system, to study the upper, the middle and the lower part of the resin bed. Figure 6a presents the evolution over time of the transverse relaxation rate $1/T_{2,slow}$ of the slowly relaxing proton fraction for the three regions of the resin bed. Figure 6b shows the evolution of the normalized amplitude A_{slow} of this fraction of protons. As expected, the saturation of the resin bed occurs first for the upper part (after 2.35 h), then for the middle part (after 3.05 h), and finally for the lower part of the resin bed (4.23 h). The same shift of the curves is observed for the evolution with time of the normalized amplitude (Figure S3) and relaxation rate (Figure S4) of the fast fraction.

As the aim of the experiment is to detect the complete saturation of the whole resin bed, we decided for the rest of the study to focus on the lower part of the column. Indeed, when this zone is saturated with paramagnetic ions, it means that the whole resin bed is saturated.

3.1.5 | Longitudinal Relaxation Rate of the Resin bed

We performed the same analysis with the T_1 relaxation curves, which are also clearly multiexponential. Typical curves are

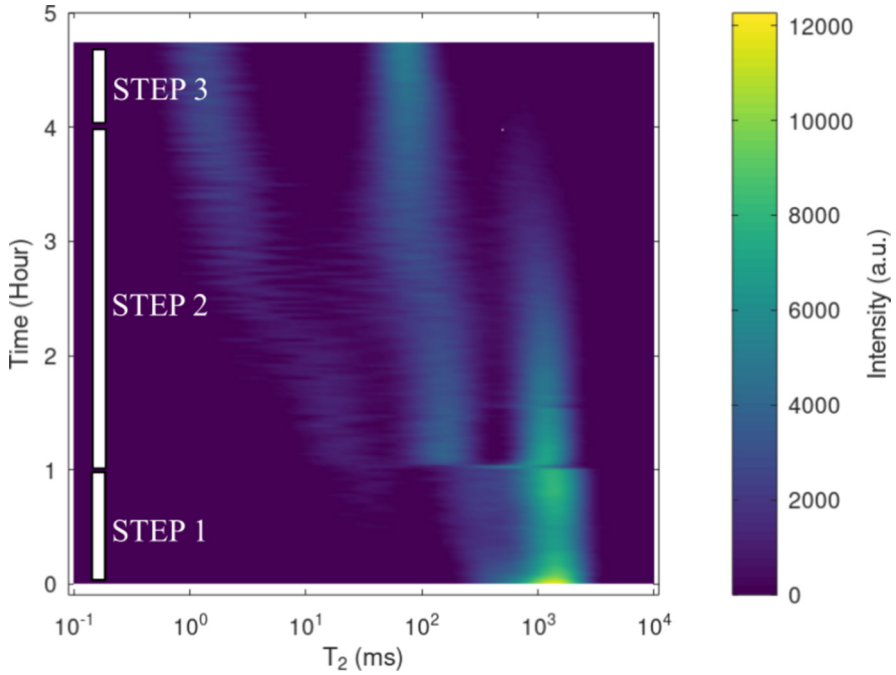

FIGURE 5 | Loading of the bottom of an IR120 resin bed with Ni^{2+} ions. T_2 distributions obtained by the inverse Laplace transform of the CPMG relaxation curves.

provided in Figure S5. However, the relative errors on the parameters (~15%) obtained by the biexponential fitting were significantly larger than for transverse relaxation curves, because of the limited number of points: 16 for an inversion recovery curve in comparison with 18,000 for a CPMG curve. With such a small number of delays, it is difficult to cover the relaxation of all the fractions present in the sample. The solution would have been to use more relaxation delays in the inversion-recovery sequence, but this would have made the measurement much too long for an accurate follow up of column saturation. Therefore, we decided to focus on transverse relaxation, which quickly provides many points for the fitting.

3.2 | Loading of a Dowex Marathon MSC Resin Bed With Ni^{2+} Ions

During the loading of a Marathon MSC resin bed with Ni^{2+}, the evolution with time of the relaxation rate and normalized amplitude of the slowly relaxing water fraction is very similar to what was observed for the IR120 resin, as shown in Figure 7a,b respectively. However, the arrival of the concentrated Ni^{2+} solution in the studied zone cannot be seen clearly as it was the case for IR120 resin (transition between steps 1 and 2 in Figure 3). This is probably because the relaxation rate of water contained in the unloaded resin is larger for Marathon MSC (~6.5 s^{-1}) than for IR120 resin (~1.8 s^{-1}). The contrast between the relaxation rate of water contained in unloaded Marathon MSC resin and the arriving Ni^{2+} solution is thus less marked than in the case of the IR120 resin. On the contrary, the transition corresponding to the saturation of the resin bed (transition between steps 2 and 3) can be easily seen in the curves. In this case, $1/T_{2,slow}$ reaches 80% of its final value after 3.3 h. After the complete saturation, $1/T_{2,slow}$ is again larger than the relaxation rate of a 20-mM Ni^{2+} solution measured in the same conditions ($1/T_2 = 12.2\,s^{-1}$).

As for the IR120 resin, this could be explained by the interporosity of the resin bed combined with differences in magnetic susceptibility between the resin beads and the flowing solution. The T_2 distributions calculated by the ILT of the transverse relaxation curves are provided in Figure S6 and confirm the interpretation. The breakthrough curve, obtained thanks to the measurement of Ni^{2+} concentration in the effluent during the experiment (Figure 8), is in good agreement with the evolution of $1/T_{2,slow}$.

The saturation thus occurs earlier for the Marathon MSC resin than for the IR120 resin, which is logical because the capacity for Ni^{2+} capture of the former resin is smaller [19].

3.3 | Loading of an Amberlite IR120 Resin Bed With Cu^{2+} Ions

The transverse relaxation rate of a 20-mM solution is two times larger for a Cu^{2+} solution than for a Ni^{2+} solution. Similarly, the relaxation of the water contained in the intraporosity of the resin is also faster for Cu^{2+}-saturated resin than for Ni^{2+}-saturated resin. Indeed, as the content of Cu^{2+}-saturated IR120 resin is ~40 $mg_{Cu}/g_{dry\ resin}$, one can estimate the T_2 value inside the Cu^{2+}-saturated resin at ~0.25 ms, using the power law of our previous study [17]. This is too fast to be detected by the CPMG sequence used in this work. Therefore, after the saturation of the resin bed (step 3), a monoexponential fitting of the relaxation curves had to be used instead of a biexponential fitting, contrarily to what was done in the case of Ni^{2+}. This choice was made according to the R^2 adjusted value that became larger for the monoexponential fitting after the saturation of the column. A typical curve of transverse relaxation after the saturation is shown in Figure S7 and proves that the monoexponential fitting is adequate. Figure 9a,b presents the evolution of the relaxation rate and the normalized amplitude of the slow fraction during the experiment. The normalized amplitude of the

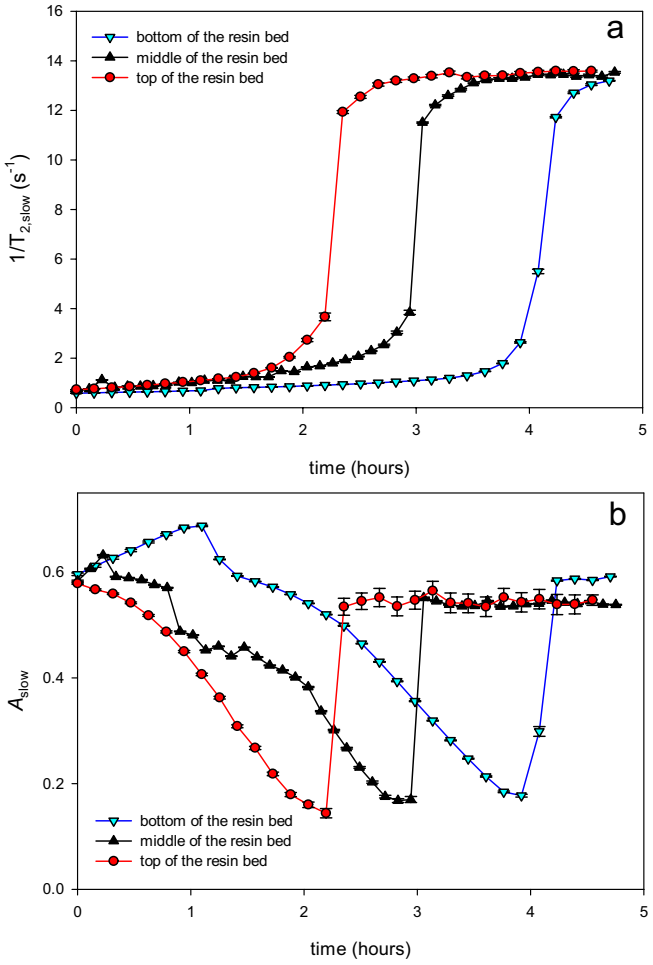

FIGURE 6 | Loading of an IR120 resin bed with Ni^{2+}. Evolution with time of (a) the transverse relaxation rate $1/T_{2,slow}$ and (b) the normalized amplitude A_{slow} of the slow fraction obtained by the biexponential fitting of the transverse relaxation data for three different heights of the studied zone of the resin bed.

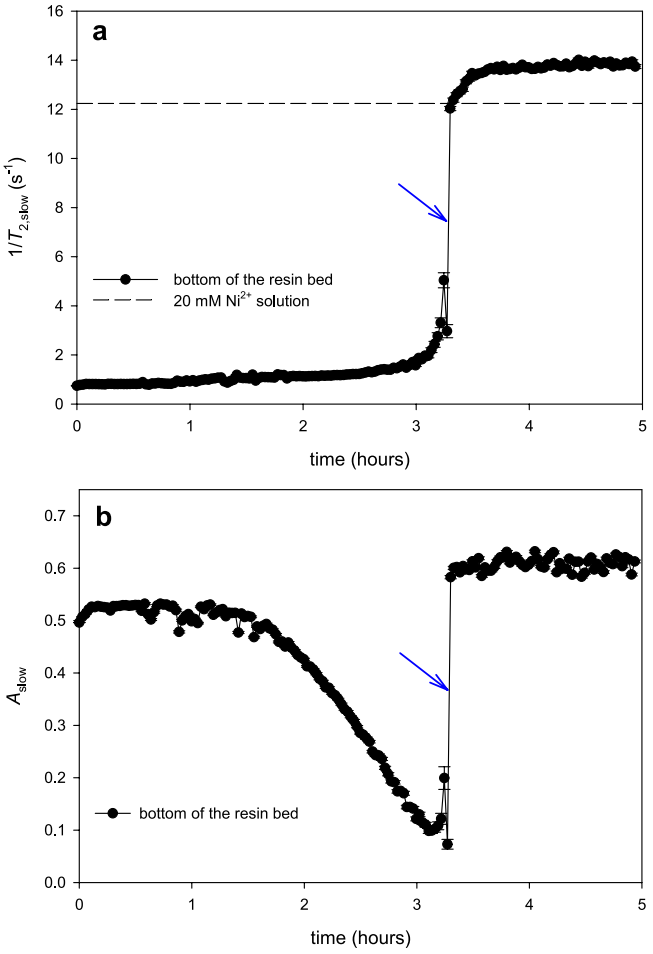

FIGURE 7 | Loading of the bottom of a Marathon MSC resin bed with Ni^{2+} ions. Evolution with time of (a) the transverse relaxation rate $1/T_{2,slow}$ of the slow fraction and (b) the normalized amplitude A_{slow} of the slow fraction obtained by the biexponential fitting of the transverse relaxation data. The blue arrow shows the transition to the saturation of the resin bed.

slow relaxing fraction of protons was put to 1 after the saturation of the column, when a monoexponential fitting was used (Figure 9b). The transition to the complete saturation of the resin bed with Cu^{2+} ions can easily be seen in Figure 9a,b after 4.41 h. As before, this value corresponds to the time when $1/T_{2,slow}$ reaches 80% of its final value. The relaxation rate of the slow fraction after saturation is close to the relaxation rate of the 20-mM Cu^{2+} solution. The relative influence of interporosity and susceptibility differences seems thus less pronounced for Cu^{2+}, probably because the initial relaxation rate of the 20-mM solution is larger for Cu^{2+} than Ni^{2+}. Interestingly, as for Ni^{2+} with the same resin, the arrival of the concentrated Cu^{2+} solution in the bottom zone of the resin bed can be observed in the curves after ~1.25 h, with a slight increase of $1/T_{2,slow}$ and decrease of A_{slow}. The analysis of the data by the ILT can be found in Figure S8. It confirms our interpretation, especially the fact that only one relaxing fraction is observed after the saturation of the resin bed.

The breakthrough curve obtained thanks to the measurement of Cu^{2+} concentration in the effluent is shown in Figure 10 and is in good agreement with the evolution of $1/T_{2,slow}$.

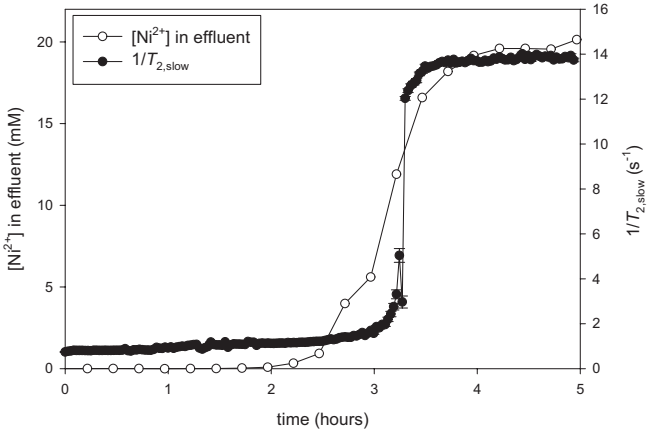

FIGURE 8 | Breakthrough curve of the Marathon MSC resin bed with a 20-mM Ni^{2+} solution, obtained by the measurement of Ni^{2+} concentration in the effluent. The evolution of $1/T_{2,slow}$ for the bottom of the resin bed is also shown for comparison.

3.4 | Loading of a Dowex Marathon Resin Bed With Cu^{2+} Ions

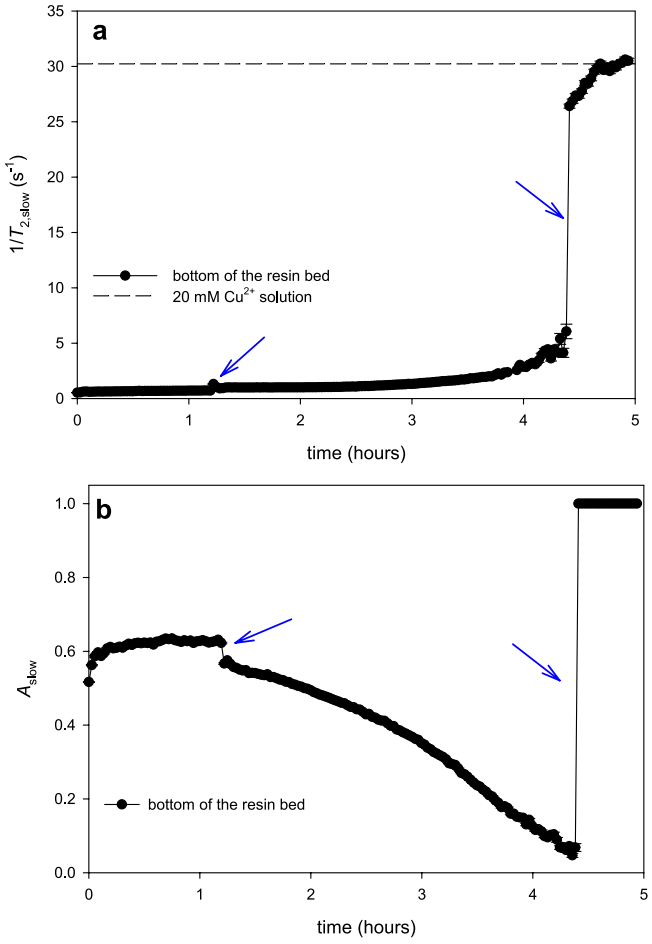

FIGURE 9 | Loading of the bottom of an IR120 resin bed with Cu^{2+} ions. Evolution with time of (a) the transverse relaxation rate $1/T_{2,slow}$ of the slow fraction and (b) the normalized amplitude A_{slow} of the slow fraction obtained by the biexponential fitting of the transverse relaxation data. The blue arrow the transition to the saturation of the resin bed.

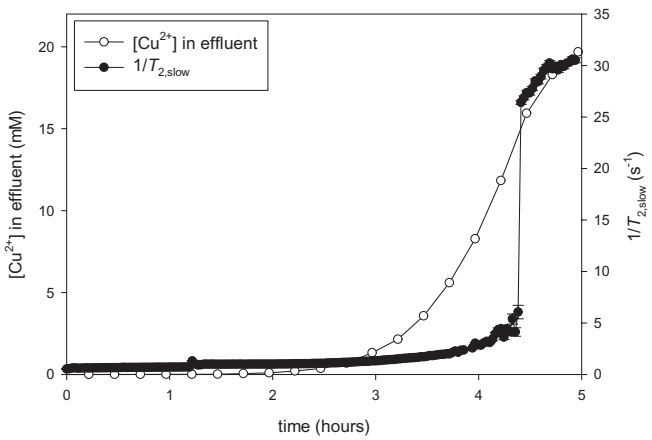

FIGURE 10 | Breakthrough curve of the IR120 resin bed with a 20-mM Cu^{2+} solution, obtained by the measurement of Cu^{2+} concentration in the effluent. The evolution of $1/T_{2,slow}$ for the bottom of the resin bed is also shown for comparison.

The results obtained for the Marathon MSC with copper ions are comparable to those obtained for the IR120 resin: after

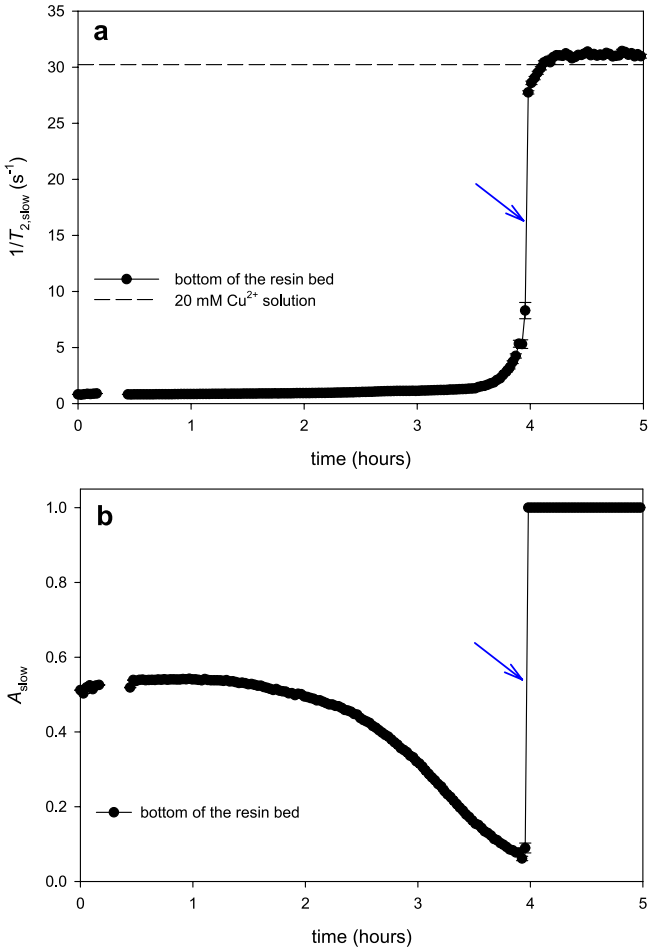

FIGURE 11 | Loading of the bottom of a Marathon MSC resin bed with Cu^{2+} ions. Evolution with time of (a) the transverse relaxation rate $1/T_{2,slow}$ of the slow fraction and (b) the normalized amplitude A_{slow} of the slow fraction obtained by the biexponential fitting of the transverse relaxation data. The blue arrow shows the transition to the saturation of the resin bed.

saturation, because of the extremely fast relaxation of the loaded resin, the relaxation becomes monoexponential with a single fraction of protons corresponding to the flowing 20-mM Cu^{2+} solution. The evolution of the amplitude and relaxation rate of the slow relaxing fraction of protons is shown in Figure 11. Data corresponding to times comprised between 0.14 and 0.44 h were removed because an uncontrolled movement of the column inside the magnet occurred during this time interval.

The T_2 distribution obtained by ILT (Figure S9) is also similar to the distribution obtained for the IR120 resin with Cu^{2+}, with a single relaxation fraction after the saturation of the column. As in the previous cases, there is a good agreement between the classical breakthrough curve and the evolution of the slow relaxation rate (Figure 12).

4 | Discussion

The results presented in this proof-of-concept study show that the loading of a resin bed with Cu^{2+} or Ni^{2+} can be followed

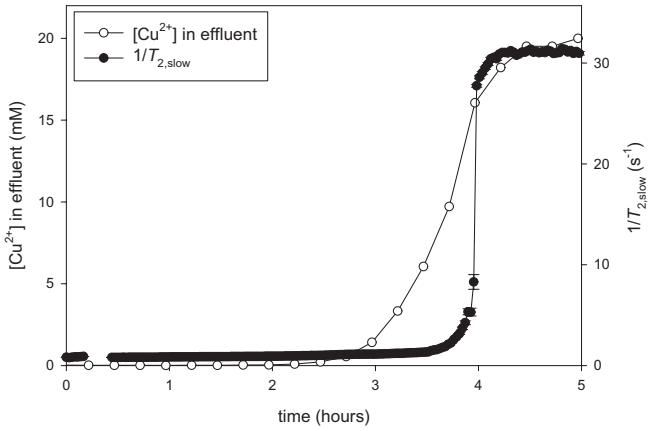

FIGURE 12 | Breakthrough curve of the Marathon MSC resin bed with a 20-mM Cu^{2+} solution, obtained by the measurement of Cu^{2+} concentration in the effluent. The evolution of $1/T_{2,slow}$ for the bottom of the resin bed is also shown for comparison.

in situ in real time with low-field NMR relaxometry. The method is noninvasive, benchtop, and does not necessitate the collection of samples. However, before any real-world application, further development is needed.

First, our interpretation is mainly based on the behavior of slowly relaxing fraction of protons of the resin bed. Indeed, we use the evolution of $1/T_{2,slow}$ to calculate the saturation time of the resin bed. Before the saturation of the column, this fraction corresponds to pure water (or water with only a small content of paramagnetic ions), but after the saturation, it corresponds to the untreated feeding solution with 20 mM of Ni^{2+} or Cu^{2+}. Our results should remain valid even with lower concentrations of paramagnetic ions, provided that the relaxation rate of the feeding solution remains significantly larger than that of water ($1/T_2 \gg 1 s^{-1}$). However, in practical applications, the concentration of the feeding solution would likely be much lower than 20 mM, with very slow relaxation, almost like that of pure water for concentrations smaller than 0.1 mM. In such cases, the raw transverse relaxation curves would differ significantly from those we obtained, which would imply to adapt their fitting and interpretation. Therefore, we plan to conduct more realistic experiments with smaller paramagnetic ion concentrations for the feeding solution. With such systems, an effective approach could be to follow the relaxation of water contained in the intraporosity of the loaded resin, rather than that of the water flowing in the interporositiy of the resin bed. Given the rapid relaxation of this fraction ($T_2 \sim 1.5$ ms for Ni^{2+} and $T_2 \sim 0.25$ ms for Cu^{2+}), the measurement sequence would need to be adapted. For instance, one could include an integration of the FID just after the excitation 90° pulse, prior to the CPMG echo train. The initial loss of the transverse relaxation curve, that is, the difference between the first point obtained with the FID and the first echo, could provide insights into the very fast relaxation of the loaded resin. Additionally, employing very short echo times could be advantageous in this context.

Second, the proposed method implies to insert the column into the bore of an NMR device, which is not easily feasible with most of conventional ion exchange columns. But with the incredible evolution of portable low field NMR [27, 28], one can reasonably imagine using a larger bore, or even a large single sided NMR sensor [29] to follow the water proton relaxation inside the column from the outside. Of course, this last step will be the most challenging because the obtained signal will not originate from the whole column but only from a zone close to the NMR sensor. Several measurements at different locations of the column may be needed to get a more accurate evaluation of the resin bed loading. The applicability of the method will also depend on the type of column: For columns contained in a metallic housing, NMR follow-up of course will not work. A too thick outer wall could also be problematic.

Finally, this work focused on Cu^{2+} and Ni^{2+}, but the method can for sure be adapted for other paramagnetic ions like Mn^{2+}, Cr^{3+}, Co^{2+}, and Fe^{2+}. However, when multiple paramagnetic ions are present in the treated water, their combined effect on transverse relaxation will be global, making it difficult to attribute the effect to a specific ion. It is also important to note that the NMR method is ineffective with diamagnetic heavy metal ions, as their presence does not influence the relaxation of water protons.

5 | Conclusion

This proof-of-concept study shows that NMR relaxometry can be used to follow the loading of ion exchange resins with Cu^{2+} and Ni^{2+} during a column experiment. The results are promising, but new experiments with smaller paramagnetic ions concentrations are needed to adapt the protocol before an application to real filtration systems.

Acknowledgments

This work was supported by FRS-FNRS (Wallonia-Brussels Federation, Belgium) grants (grant numbers T.0113.20, CDR J.0093.22 and CDR J.0025.15). The authors acknowledge Anne-Lise Hantson for helpful discussion about column experiments.

References

1. O. B. Akpor, "Heavy Metal Pollutants in Wastewater Effluents: Sources," *Effects and Remediation, Advances in Bioscience and Bioengineering* 2 (2014): 37, https://doi.org/10.11648/j.abb.20140204.11.

2. P. B. Tchounwou, C. G. Yedjou, A. K. Patlolla, and D. J. Sutton, "Heavy Metals Toxicity and the Environment," *EXS* 101 (2012): 133–164, https://doi.org/10.1007/978-3-7643-8340-4_6.

3. S. K. Sharma, *Heavy Metals in Water: Presence, Removal and Safety* (Cambridge: The Royal Society of Chemistry, 2014), https://doi.org/10.1039/9781782620174.

4. World Health Organization, *Guidelines for Drinking-Water Quality: Fourth Edition Incorporating First Addendum*, 4th ed + 1st add ed. (Geneva: World Health Organization, 2017), https://iris.who.int/handle/10665/254637.

5. F. Fu and Q. Wang, "Removal of Heavy Metal Ions From Wastewaters: A Review," *Journal of Environmental Management* 92 (2011): 407–418, https://doi.org/10.1016/j.jenvman.2010.11.011.

6. R. Rao and H. A. L. Gadde, "Heavy Metal Adsorption by Hydrous Iron and Manganese Oxides," *Analytical Chemistry* 46 (1974): 2022–2026, https://doi.org/10.1021/ac60349a004.

7. L. Monser and N. Adhoum, "Modified Activated Carbon for the Removal of Copper, Zinc, Chromium and Cyanide From Wastewater," *Separation and Purification Technology* 26 (2002): 137–146, https://doi.org/10.1016/S1383-5866(01)00155-1.

8. M. Muchie and O. B. Akpor, "Remediation of Heavy Metals in Drinking Water and Wastewater Treatment Systems: Processes and Application," *International Journal of Physical Science* 5 (2010): 1807–1817.

9. L. Banci, I. Bertini, and C. Luchinat, *Nuclear and Electron Relaxation: The Magnetic Nucleus-Unpaired Electron Coupling in Solution* (Weinheim: Wiley-VCH, 1991).

10. F. V. C. Kock, M. P. Machado, G. P. B. Athayde, L. A. Colnago, and L. L. Barbosa, "Quantification of Paramagnetic Ions in Solution Using Time Domain NMR. PROS and CONS to Optical Emission Spectrometry Method," *Microchemical Journal* 137 (2018): 204–207, https://doi.org/10.1016/j.microc.2017.10.013.

11. A. B. Moradi, S. E. Oswald, J. A. Massner, K. P. Pruessmann, B. H. Robinson, and R. Schulin, "Magnetic Resonance Imaging Methods to Reveal the Real-Time Distribution of Nickel in Porous Media," *European Journal of Soil Science* 59 (2008): 476–485, https://doi.org/10.1111/j.1365-2389.2007.00999.x.

12. J. Bartacek, F. J. Vergeldt, J. Maca, E. Gerkema, H. Van As, and P. N. L. Lens, "Iron, Cobalt, and Gadolinium Transport in Methanogenic Granules Measured by 3D Magnetic Resonance Imaging," *Frontiers in Environmental Science* 4 (2016): 13, https://doi.org/10.3389/fenvs.2016.00013.

13. N. Nestle, T. Baumann, A. Wunderlich, and R. Niessner, "MRI Observation of Heavy Metal Transport in Aquifer Matrices Down to Sub-mg Quantities," *Magnetic Resonance Imaging* 21 (2003): 345–349.

14. N. Nestle, M. Ebert, A. Wunderlich, and B. Thomas, "Long-Term Observation of Adsorbed Heavy Metal Ions in Sediment Samples by MRI," *Diffusion Fundamentals* 5 (2007): 7.1–7.19.

15. A. Greiner, W. Schreiber, G. Brix, and W. Kinzelbach, "Magnetic Resonance Imaging of Paramagnetic Tracers in Porous Media: Quantification of Flow and Transport Parameters," *Water Resources Research* 33 (1997): 1461–1473, https://doi.org/10.1029/97WR00657.

16. Y. Gossuin and Q. L. Vuong, "NMR Relaxometry for Adsorption Studies: Proof of Concept With Copper Adsorption on Activated Alumina," *Separation and Purification Technology* 202 (2018): 138–143, https://doi.org/10.1016/j.seppur.2018.03.051.

17. Y. Gossuin, A.-L. Hantson, and Q. L. Vuong, "Low Resolution Benchtop Nuclear Magnetic Resonance for the Follow-Up of the Removal of Cu^{2+} and Cr^{3+} From Water by Amberlite IR120 ion Exchange Resin," *Journal of Water Process Engineering* 33 (2020): 101024, https://doi.org/10.1016/j.jwpe.2019.101024.

18. S. Marchesi, S. Nascimbene, M. Guidotti, C. Bisio, and F. Carniato, "Application of NMR Relaxometry for Real-Time Monitoring of the Removal of Metal Ions From Water by Synthetic Clays," *Dalton Transactions* 51 (2022): 4502–4509, https://doi.org/10.1039/D1DT04344G.

19. M. Bernardi, A.-L. Hantson, G. Caulier, et al., "Ni^{2+} Removal by Ion Exchange Resins and Activated Carbon: A Benchtop NMR Study," *International Journal of Environmental Science and Technology* 21 (2024): 8337–8360, https://doi.org/10.1007/s13762-024-05547-2.

20. O. Hamdaoui, "Removal of Copper (II) From Aqueous Phase by Purolite C100-MB Cation Exchange Resin in Fixed bed Columns: Modeling," *Journal of Hazardous Materials* 161 (2009): 737–746, https://doi.org/10.1016/j.jhazmat.2008.04.016.

21. L.-C. Lin, J.-K. Li, and R.-S. Juang, "Removal of Cu(II) and Ni(II) From Aqueous Solutions Using Batch and Fixed-Bed ion Exchange Processes," *Desalination* 225 (2008): 249–259, https://doi.org/10.1016/j.desal.2007.03.017.

22. N. H. Shaidan, U. Eldemerdash, and S. Awad, "Removal of Ni(II) Ions From Aqueous Solutions Using Fixed-Bed ion Exchange Column Technique," *Journal of the Taiwan Institute of Chemical Engineers* 43 (2012): 40–45, https://doi.org/10.1016/j.jtice.2011.06.006.

23. N. Dizge, B. Keskinler, and H. Barlas, "Sorption of Ni(II) Ions From Aqueous Solution by Lewatit Cation-Exchange Resin," *Journal of Hazardous Materials* 167 (2009): 915–926, https://doi.org/10.1016/j.jhazmat.2009.01.073.

24. M. C. D. Tayler and D. Sakellariou, "Low-Cost, Pseudo-Halbach Dipole Magnets for NMR," *Journal of Magnetic Resonance* 277 (2017): 143–148, https://doi.org/10.1016/j.jmr.2017.03.001.

25. A. T. Watson and C. T. P. Chang, "Characterizing Porous Media With NMR Methods," *Progress in Nuclear Magnetic Resonance Spectroscopy* 31 (1997): 343–386, https://doi.org/10.1016/S0079-6565(97)00053-8.

26. S. W. Provencher, "A Constrained Regularization Method for Inverting Data Represented by Linear Algebraic or Integral Equations," *Computer Physics Communications* 27 (1982): 213–227, https://doi.org/10.1016/0010-4655(82)90173-4.

27. E. Torres, P. Wang, S. Kantesaria, et al., "Development of a Compact NMR System to Measure pO_2 in a Tissue-Engineered Graft," *Journal of Magnetic Resonance* 357 (2023): 107578, https://doi.org/10.1016/j.jmr.2023.107578.

28. J. Marreiros, R. De Oliveira-Silva, P. Iacomi, P. L. Llewellyn, R. Ameloot, and D. Sakellariou, "Benchtop *In Situ* Measurement of Full Adsorption Isotherms by NMR," *Journal of the American Chemical Society* 143 (2021): 8249–8254, https://doi.org/10.1021/jacs.1c03716.

29. R. de Oliveira-Silva, É. Lucas-Oliveira, A. G. de Araújo-Ferreira, et al., "A Benchtop Single-Sided Magnet With NMR Well-Logging Tool Specifications—Examples of Application," *Journal of Magnetic Resonance* 322 (2021): 106871, https://doi.org/10.1016/j.jmr.2020.106871.

Supporting Information

Additional supporting information can be found online in the Supporting Information section.